Estimates of fluvial erosion on Titan from sinuosity of lake shorelines

Yodit Tewelde,[1] J. Taylor Perron,[1] Peter Ford,[2] Scott Miller,[1,3] and Benjamin Black[1]

Received 21 June 2013; revised 5 August 2013; accepted 7 September 2013; published 22 October 2013.

[1] Titan has few impact craters, suggesting that its surface is geologically young. Titan's surface also has abundant landforms interpreted to be fluvial networks. Here we evaluate whether fluvial erosion has caused significant resurfacing by estimating the cumulative erosion around the margins of polar lakes. A scarcity of detailed topographic data makes it difficult to measure fluvial incision on Titan, but images of drowned fluvial features around the lake margins, where elevated levels of hydrocarbon liquids appear to have partly flooded fluvial valleys, offer a constraint on the topography. We mapped the shorelines of several lakes to obtain topographic contours that trace the fluvially dissected topography. We then used a numerical landscape evolution model to calibrate a relationship between contour sinuosity, which reflects the extent of fluvial valley incision, and cumulative erosion. We confirmed this relationship by analyzing a partially dissected surface adjacent to the Minnesota River, USA. Comparison of the mapped Titan contours with the sinuosity-erosion relationship suggests that cumulative fluvial erosion around the margins of Titan's polar lakes, including Ligeia Mare, Kraken Mare, and Punga Mare in the north and Ontario Lacus in the south, ranges from 4% to 31% of the initial relief. Additional model simulations show that this amount of fluvial erosion does not render craters invisible at the resolution of currently available imagery, suggesting that fluvial erosion is not the only major resurfacing mechanism operating in Titan's polar regions.

Citation: Tewelde, Y., J. T. Perron, P. Ford, S. Miller, and B. Black (2013), Estimates of fluvial erosion on Titan from sinuosity of lake shorelines, *J. Geophys. Res. Planets*, *118*, 2198–2212, doi:10.1002/jgre.20153.

1. Introduction

[2] Images from the Descent Imager/Spectral Radiometer (DISR) on the Huygens Probe and the Synthetic Aperture Radar (SAR) instrument on the Cassini spacecraft have revealed extensive fluvial networks in many regions on Titan [*Tomasko et al*., 2005; *Soderblom et al*., 2007; *Lorenz et al*., 2008; *Burr et al*., 2009, 2013; *Langhans et al*., 2012; O. Aharonson et al., Titan's surface geology, submitted to *Titan: Surface, Atmosphere and Magnetosphere*, edited by I. Mueller-Wodarg et al., 384 pp., Cambridge Univ. Press, Cambridge, U.K., 2013], some of which drain into lakes near the north and south poles [*Mitri et al*., 2007; *Stofan et al*., 2007]. Titan appears to be the only body in the Solar System other than Earth where rivers have recently flowed on the surface. Unlike Earth, however, Titan has rivers of liquid methane and ethane incising into a surface of water ice and organic sediments [*Griffith et al*., 2003], and river valleys near the poles feed into lakes of methane, ethane, and other hydrocarbons [*Stofan et al*., 2007]. No river channels have been observed directly on Titan due to the coarse image resolution, but the observed landforms are interpreted to be fluvial valleys based on their morphology and context, which are similar to features on Earth that were formed mechanically by surface runoff [*Perron et al*., 2006; *Aharonson* et al., submitted manuscript, 2013; *Burr et al*., 2013]. In addition, methane comprises several percent of Titan's atmosphere, and the surface conditions allow methane to exist as a gas or a liquid [*Niemann et al*., 2005]. All of this suggests that Titan has a methane cycle that is analogous to Earth's water cycle.

[3] This high concentration of atmospheric methane presents a puzzle, because methane undergoes photochemical breakdown that limits its atmospheric lifetime to 10–100 Myr [*Niemann et al*., 2005]. To sustain the observed methane concentration over billions of years, there must be a source of replenishment [*Yung et al*., 1984]. It is possible that a transfer of subsurface material to the surface and atmosphere could be responsible for the methane replenishment [*Lunine and Lorenz*, 2009; *Lopes et al*., 2013].

[4] However, the geological processes operating on Titan remain an outstanding problem, in part because of questions regarding the history of Titan's surface. Cassini observations have revealed only a few scattered impact craters, which indicate a relatively young surface that is estimated to be between a few hundred million years and 1 Gyr old [*Lorenz et al*., 2007; *Wood et al*., 2010; *Neish and Lorenz*, 2012]. Several plausible resurfacing mechanisms could potentially help to explain this young surface, including cryovolcanism [*Sotin et al*., 2005; *Lopes et al*., 2007a, 2013], tectonic

[1]Department of Earth, Atmospheric and Planetary Sciences, Massachusetts Institute of Technology, Cambridge, Massachusetts, USA.
[2]Kavli Institute for Astrophysics and Space Research, Massachusetts Institute of Technology, Cambridge, Massachusetts, USA.
[3]Department of Earth and Environmental Sciences, University of Michigan, Ann Arbor, Michigan, USA.

Corresponding author: J. T. Perron, Department of Earth, Atmospheric and Planetary Sciences, Massachusetts Institute of Technology, Cambridge, MA 02139, USA. (perron@mit.edu)

©2013. American Geophysical Union. All Rights Reserved.
2169-9097/13/10.1002/jgre.20153

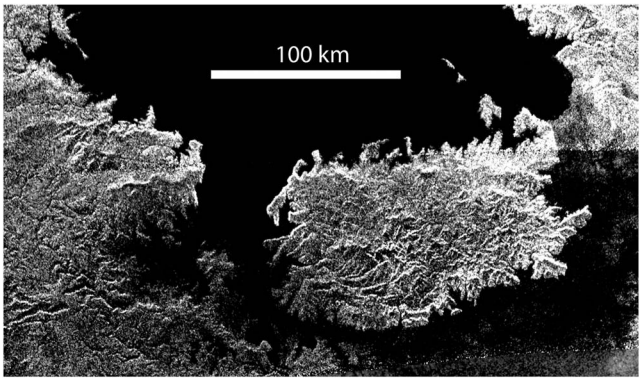

Figure 1. SAR image of Kraken Mare shoreline at approximately 78°N, 60°E. Illumination direction is from the top of the image. Pixel values represent normalized radar cross section σ_0 in decibels, from −20 dB (black) to +0 dB (white). The large peninsula or island is Mayda Insula. The sharp contrast between the dark lake and the rough, lighter surrounding terrain traces out a topographic contour through a fluvially dissected landscape that appears to have been partially flooded by a rising lake level.

deformation [*Radebaugh et al*., 2007], organic aerosol deposition [*McKay et al*., 2001], dune migration and Aeolian deposition [*Radebaugh et al*., 2008], and widespread erosional denudation [*Black et al*., 2012]. Determining which of these processes are significant is essential to understanding Titan's geologic history and thus Titan's interior processes and hydrocarbon cycle.

[5] The purpose of this paper is to assess the extent of resurfacing by fluvial erosion on Titan, particularly in the vicinity of the polar lakes. On Earth, rates and amounts of fluvial erosion can be estimated by a combination of three-dimensional topographic measurements, field observations, and geochronologic techniques that require field sampling [*Bierman*, 1994; *Black et al*., 2012; *Ferrier et al*., 2013b]. On Titan, we are currently unable to directly measure rates or amounts of landscape change. The Cassini-Huygens mission was not designed to perform widespread topographic mapping, but a limited set of topographic measurements has been obtained from a combination of radar altimetry [*Elachi et al*., 2004], stereogrammetry of overlapping SAR swaths [*Kirk et al*., 2008, 2009], and a technique known as SARTopo that uses the overlapping returns of the radar instrument's multiple beams [*Stiles et al*., 2009]. However, these basic digital elevation models (DEMs) are rare, covering a small fraction of Titan's surface. Although the acquisition of such data is an impressive technical feat [*Radebaugh et al*., 2007; *Soderblom et al*., 2007; *Stiles et al*., 2009], the resolution, precision, and coverage are generally not sufficient for measurements of the width, depth, or cross-sectional form of individual fluvial valleys or of the surrounding hillslopes. Moreover, precise measurements of the present topography would be insufficient to measure cumulative erosion without additional constraints on the initial topography. Thus, it is not clear whether Titan's landscape is the result of steady, protracted, and significant exhumation of its crust (over perhaps billions of years) or only minimal, recent fluvial incision and hillslope adjustment.

[6] In the absence of adequate knowledge of the initial and present topography of the fluvially dissected landscape, alternative approaches must be employed to estimate how much erosion has occurred. *Black et al*. [2012] developed a procedure for estimating the spatially averaged cumulative erosion of a surface, as a fraction of the initial topographic relief, by measuring the map view geometry of drainage networks. They studied fluvial networks in SAR images covering two north polar areas, one equatorial area, and one south polar area. Drainage networks in all four areas are consistent with minimum erosion of 0.4% of initial relief. Two of the regions yielded estimates of maximum erosion (9% for one of the north polar areas and 16% for the south polar area), but these upper bounds were less certain than the lower bounds, and the remaining two sites did not yield well-defined upper bounds. The study by *Black et al*. [2012] implies that some areas of Titan's surface have experienced relatively little erosion since the most recent resurfacing event, but it is not clear how extensive these areas are. To address some of these questions and extend our understanding of fluvial processes on Titan, we seek to obtain additional estimates of regional erosion using independent techniques.

[7] Despite the lack of topographic data sets that resolve individual fluvial valleys, there are some surface features on Titan that delineate fluvial topography and are visible in images. The polar lakes provide a two-dimensional imprint of Titan's three-dimensional fluvial topography at a level of detail that is otherwise inaccessible with current data. SAR images reveal elevated levels of hydrocarbon liquids in some of the polar lakes, which have partly flooded fluvial valleys around the lake margins, similar to ria shorelines on Earth (Figure 1) [*Stofan et al*., 2007; *Wasiak et al*., 2013]. If each lake level is a surface of constant gravitational potential, the imaged shoreline is an elevation contour with a shape that reflects the dissection of the surrounding landscape.

[8] Geomorphological studies on Earth (and even on Mars) typically make use of abundant topographic data, so there is no established procedure for estimating erosion from a single elevation contour. In this paper, we describe such a procedure and use it to obtain estimates of cumulative erosion in the vicinity of Titan's polar lakes. In section 2, we provide an overview of current knowledge about Titan's polar lakes and the associated fluvial features. In section 3, we use a simple numerical landscape evolution model to calibrate a relationship between the sinuosity of an elevation contour surrounding a topographic depression and the average amount of cumulative fluvial erosion of the surrounding landscape. We test this relationship in section 4 by applying it to a terrestrial landscape, a partly dissected plateau where cumulative erosion and contour sinuosity can both be measured, and confirm that contour sinuosity provides useful estimates of erosion. In section 5, we map the shorelines around several polar lakes on Titan, measure the sinuosity of these shorelines, and use the model-derived relationship to estimate the cumulative fluvial erosion around the margins of Titan's polar lakes.

2. Titan's Polar Lakes

[9] While Titan's current conditions allow for liquid methane anywhere on its surface, only the highest latitudes have relative humidity levels at which bodies of liquid methane are expected to persist without evaporating [*Stofan et al*., 2007]. *Stofan et al*. [2007] reported the first hydrocarbon lakes observed by Cassini RADAR, and as of this writing, with 55.4% of Titan's surface imaged by SAR, 655 lake features from $<10\,km^2$ to $>100{,}000\,km^2$ have been

identified, all of which are poleward of 55° latitude, with most at high northern latitudes [*Aharonson* et al., submitted manuscript, 2013]. The formation processes of the original lake depressions are still unknown, but possible mechanisms include impact cratering [*Stofan et al*., 2007], cryovolcanic caldera collapse [*Lopes et al.*, 2007a], karst-like dissolution [*Lopes et al*., 2007b; *Mitchell et al*., 2008], or tectonic opening of structural basins [*Wall et al*., 2010]. Alternatively, hydrocarbon liquids may have simply filled local depressions on a rough surface. Three types of lake shorelines are observed [*Stofan et al*., 2007; *Hayes et al*., 2008]. Lakes of the first type have sharply defined, rounded shorelines with no associated channel networks visible. These may be fed only by subsurface flow of hydrocarbons, though it is impossible to rule out the possibility that surface drainage networks are present, given the currently available image resolution [*Burr et al*., 2013]. Lakes of the second type have more distinctly polygonal shapes with rough shoreline geometries and appear to be fed by fluvial networks. Lakes of the third type are similar to the second type, in that they are clearly associated with fluvial networks, but portions of the lake margins where fluvial features terminate have a branching shape that suggests that rising lake levels have flooded river valleys that eroded when lake levels were lower [*Stofan et al*., 2007; *Hayes et al*., 2008; *Wall et al*., 2010; *Aharonson* et al., submitted manuscript, 2013; *Wasiak et al*., 2013]. This third class of lakes is the focus of our study.

[10] A pronounced hemispherical asymmetry has been observed between the northern polar region, where roughly 10% of the imaged surface area is covered by lakes [*Aharonson* et al., submitted manuscript, 2013] and southern polar region, which is largely devoid of lakes [*Aharonson et al*., 2009]. *Aharonson et al*. [2009] suggest that this observation can be explained by a combination of Titan's 29.5 year seasonal cycle and an asymmetry in the seasons due to Saturn's axial obliquity and orbital eccentricity, somewhat similar to the effects of Earth's Milankovitch cycles on Pleistocene glaciations. Currently, lake levels in the northern polar region appear to be rising, while observations of Ontario Lacus suggest that lake levels in the southern polar region are falling [*Barnes et al*., 2009; *Moriconi et al*., 2010; *Wall et al*., 2010; *Hayes et al*., 2011; *Turtle et al*., 2011b]. Since Cassini's arrival in 2004, Titan has progressed from southern summer to early southern autumn and from northern winter to early northern spring [*Turtle et al*., 2011a]. Continued study may reveal whether, and by how much, lake levels vary over seasonal time scales [*Lunine and Lorenz*, 2009], providing insight into Titan's methane cycle.

[11] Several previous studies have discussed the morphology of Titan's lake shores and the processes that appear to be shaping them. *Wall et al*. [2010] reported evidence of several processes modifying the margins of Ontario Lacus, including wave-driven erosion and sediment transport, river delta construction, and possibly regional tilting, but concluded that the overall form suggests a drowned coast that includes flooded fluvial valleys. *Cornet et al*. [2012], drawing an analogy to lakes in semiarid regions on Earth, additionally suggest that the margins of Ontario Lacus could have been modified by dissolution, though the solubility of Titan's surface materials in hydrocarbons remains uncertain [*Lorenz and Lunine*, 1996]. *Sharma and Byrne* [2010, 2011] compared lake shapes on Titan and Earth, as measured by fractal dimension, shoreline development index (the ratio of the shoreline perimeter to the circumference of a circle with the same area), and an elongation factor, in an effort to identify the geological processes that formed Titan's lakes. Although they determined that certain formation mechanisms do produce statistically distinct shapes on Earth, they found that Titan's distribution of lake shapes is consistent with multiple formation mechanisms.

[12] Given the evidence that multiple processes may have modified the shorelines of some of Titan's lakes, we focus our analysis on a small number of large, well-resolved lakes with shoreline morphologies that appear to be dominated by flooded river valleys. Before turning to measurements of lake shorelines on Titan, however, we seek a general relationship between the shape of a flooded lake shoreline and the extent of fluvial erosion that occurred along the lake margins prior to the rise in the lake level.

3. Landscape Evolution Model

[13] The valley networks that surround Titan's polar lakes have formed by erosion into the icy surface [*Burr et al*., 2013] by two general processes: fluvial incision and hillslope erosion [e.g., *Black et al*., 2012]. We use a simple model that incorporates these two processes [*Perron et al*., 2008a, 2009, 2012], which has previously been applied to Titan [*Black et al*., 2012], to investigate the relationship between erosion of a rough initial surface and the sinuosity of contour lines around the lake margins that define the landscape's base level.

3.1. Fluvial Incision

[14] The governing equation for the model is based on the conservation of mass of the erodible substrate, conservation of mass of the fluid that runs off of the surface and flows through the channels, and expressions describing the rate of erosion of the land surface. Some tropical valleys on Titan appear to be broad and multithreaded, suggesting that they have dominantly alluvial river beds surrounded by floodplains that may store significant volumes of sediment [*Le Gall et al*., 2010; *Burr et al*., 2013]. Topographic measurements show that other rivers have steep-sided, narrow-floored valleys inset into the surrounding terrain [*Tomasko et al*., 2005; *Soderblom et al*., 2007; *Jaumann et al*., 2008; *Kirk et al*., 2008, 2009; *Aharonson* et al., submitted manuscript, 2013; *Burr et al*., 2013], which suggests that they have incised into the surface and transported the resulting sediment downstream. The characteristics of the polar networks studied here are consistent with the latter category [*Black et al*., 2012; *Burr et al*., 2013], and a previous study of finer-scale fluvial networks near the Huygens landing site found evidence that channel incision occurs through mechanical erosion driven by runoff [*Perron et al*., 2006]. We therefore assume that the rate of fluvial incision in the polar regions is limited by the rate at which the channelized flows can detach cohesive material from the channel bed, rather than the rate at which the flows can transport channel bed sediment and any sediment delivered to the channel from surrounding hillslopes. We also assume that all eroded material is transported downstream and deposited in lakes, rather than aggrading in channels.

[15] Theoretical analyses have demonstrated that despite considerable differences in materials and physical parameters between Titan and Earth, the mechanisms that drive channel incision and sediment transport on Earth should also be effective on Titan [*Collins*, 2005; *Burr et al*., 2006]. Following models

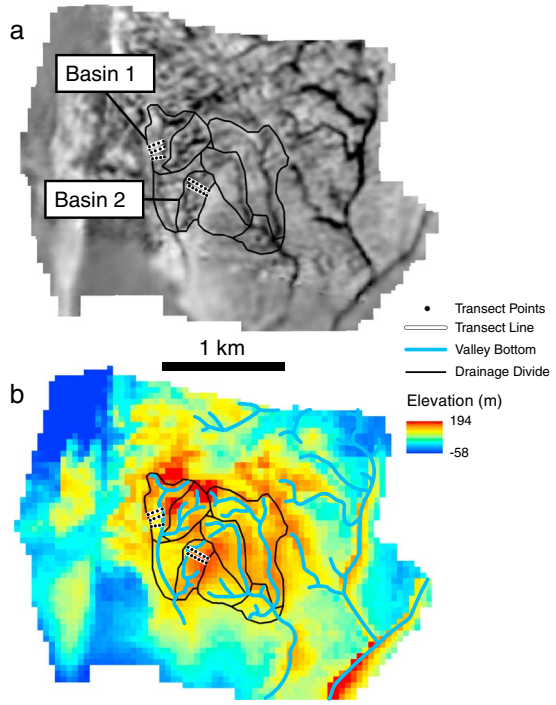

Figure 2. (a) Orthoimage based on Descent Imager/Spectral Radiometer images of an elevated area near the Huygens Probe landing site. Superimposed maps show drainage divides and hillslope transects in the portion of the image analyzed here. (b) Digital elevation model with color representing elevation relative to an arbitrary datum. Superimposed maps are the same as in Figure 2a, but with the addition of valleys mapped from the orthoimage. Data from *Soderblom et al.* [2007].

for detachment-limited fluvial incision on Earth [*Howard and Kerby*, 1983; *Howard*, 1994; *Howard et al.*, 1994; *Whipple et al.*, 2000] and supporting field observations [*Ferrier et al.*, 2013a], the rate of channel incision in our model is set to be linearly proportional to the rate of energy expenditure by the flow or "stream power" [*Seidl and Dietrich*, 1992; *Howard*, 1994; *Whipple and Tucker*, 1999]:

$$\frac{\partial z}{\partial t} = KA^m|\nabla z| \tag{1}$$

where z is elevation, t is time, A is the drainage area, $|\nabla z|$ is the magnitude of the topographic gradient (that is, the dimensionless surface slope), and K is a coefficient that depends on substrate erodibility, precipitation rates, channel cross-sectional geometry, and runoff efficiency. The exponent m describes how fluid discharge and channel geometry vary downstream and therefore influences the concavity of longitudinal channel elevation profiles. This simple model of fluvial incision is similar to the approach used to describe river incision into bedrock in numerous other models of landscape evolution [*Howard*, 1994; *Tucker and Slingerland*, 1996; *Pelletier*, 2004; *Willgoose*, 2005; *Tucker and Hancock*, 2010].

3.2. Hillslope Erosion

[16] As channel beds lower, they steepen the adjacent hillslopes, driving erosion of the surrounding landscape. The response of hillslopes to this steepening depends on the nature of the surface material. Possible hillslope configurations include a "bedrock" surface that is mantled with regolith, a surface of exposed bedrock with no regolith cover, or a thick deposit of granular material. Images from the Huygens landing site show abundant, rounded granular material covering the ground surface [*Tomasko et al.*, 2005], but it is unknown how thick this granular layer is or whether this is representative of Titan's surface in other locations. These different hillslope types will respond differently to channel incision and could develop distinct topographic profiles. If the hillslopes are mantled with or consist entirely of cohesionless, granular material, slopes should be at the angle of repose or lower. If the hillslopes consist of exposed bedrock or some other material with significant cohesion, then slope angles may be steeper than the angle of repose.

[17] In the absence of detailed observations of the hillslopes surrounding channel networks on Titan, we use

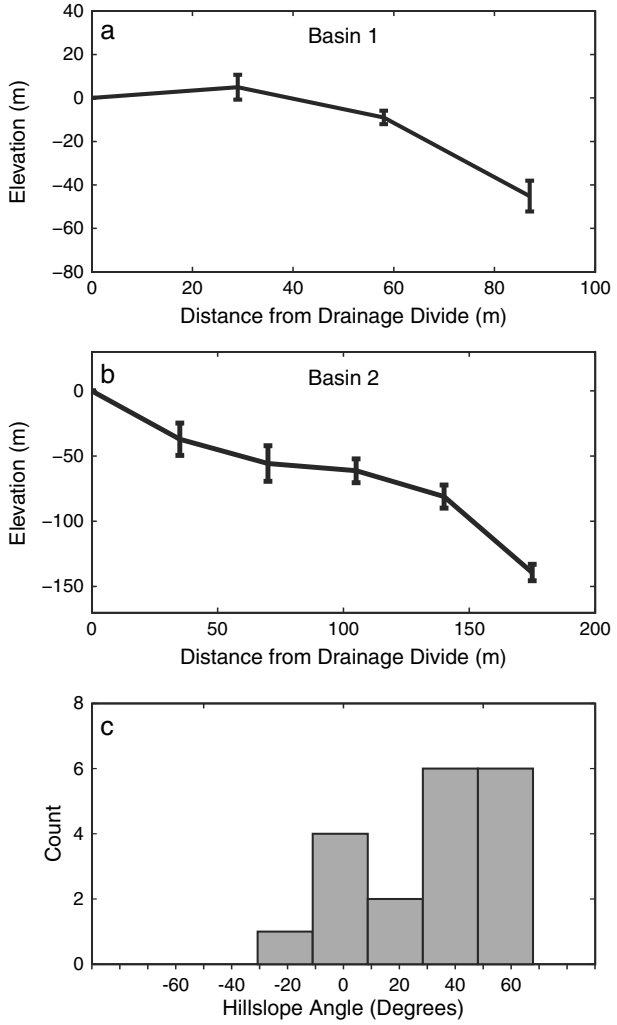

Figure 3. Average hillslope profiles extracted from Huygens stereo topography at the locations shown in Figure 2 for (a) Basin 1 and (b) Basin 2. Points are average elevations obtained by binning multiple adjacent hillslope profiles, with error bars denoting the standard error of the mean of each bin. (c) Histogram of individual slope measurements from all profiles. Negative slopes correspond to sections of profiles that slope in a direction opposite to that expected from the overall valley shape.

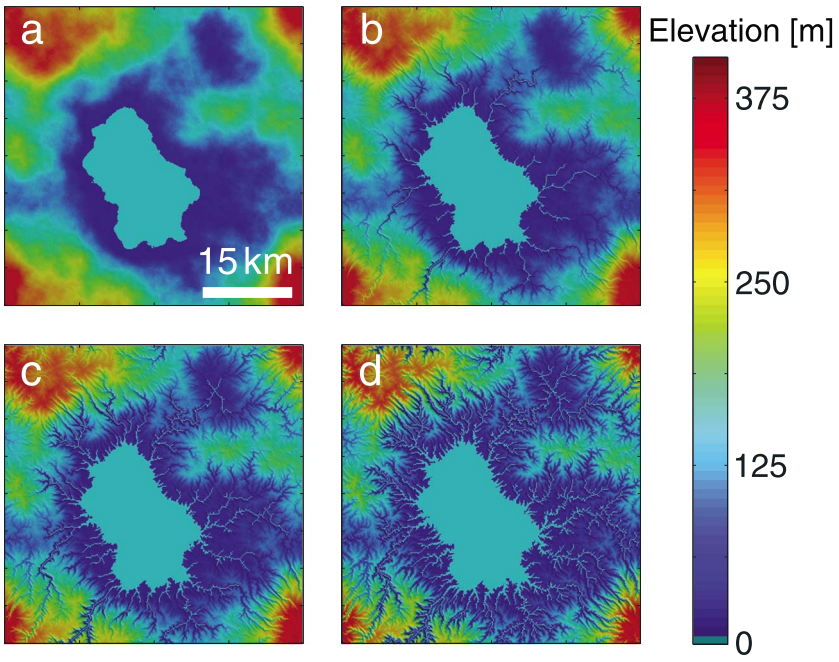

Figure 4. Shaded relief maps of topographic surfaces at four instants in a representative landscape evolution model simulation. Color indicates relative elevation. Normalized cumulative erosion amounts E/H_0 are (a) 0, (b) 0.10, (c) 0.20, and (d) 0.50.

the few available hillslope profiles near the Huygens landing site to constrain the hillslope response to channel incision. The DISR instrument onboard the Huygens probe returned the highest-resolution images of Titan's surface (< 20 m/pixel). A 50 m/pixel digital elevation model (DEM) and corresponding 12.5 m/pixel orthophotos covering an area of approximately 3 by 5 km were generated from six overlapping DISR stereo pairs [*Soderblom et al.*, 2007] (Figure 2). We identified valley bottoms as linear features that appear dark in the images and ridgelines as intervening topographic highs that lie between valley heads. We then extracted hillslope profiles in the two drainage basins where the mapped valleys correspond to topographic lows in the DEM and where valley side slopes were long enough for several elevation measurements to be taken between a drainage divide and valley bottom. Elevations were interpolated linearly from the four nearest points in the DEM. In order to extract representative hillslope shapes from the noisy DEM data, multiple adjacent profiles within each valley were binned to generate average hillslope profiles (Figures 3a–3b).

[18] The average profiles (Figures 3a–3b) and the distribution of all slope measurements (Figure 3c) show that slopes are typically about 30° (median 31°, 95% confidence interval 17° to 51°) but vary widely, with several measurements steeper than 60°. Experiments indicate that static friction angles for sand and gravel under reduced gravity can be up to 5° higher than terrestrial values and dynamic friction angles up to 10° lower [*Kleinhans et al.*, 2011], suggesting that friction angles for cohesionless material on Titan may lie between 20° and 36°. Although the small number of negative slopes in Figure 3c suggests that there may be significant uncertainties in the DISR elevations, and hence slope estimates, the large number of steep slopes and the truncation of the distribution at approximately 60° are consistent with the hypothesis that many of the hillslopes in the DISR images equal or exceed the friction angles for cohesionless material. This observation suggests that hillslope surfaces near the Huygens landing site consist of either exposed bedrock or sediment at a critical angle and that hillslope erosion keeps pace with fluvial incision through oversteepening that leads to hillslope failure [*Binnie et al.*, 2007]. Given these measurements, we incorporate mass wasting as the dominant hillslope erosion mechanism in the model. This is implemented as a simple rule: When slopes surpass a threshold gradient of 0.6, failure occurs and material is eroded (and transported out of the system) until the gradient returns to the threshold value [*Tucker and Slingerland*, 1994; *Pelletier*, 2004]. At the spatial scales of interest (tens of kilometers), neither the specific threshold gradient nor the hillslope erosion law in general has a strong effect on drainage network development [*Tucker and Slingerland*, 1996].

3.3. Initial Surface and Simulation Procedure

[19] The initial terrain is a random, autocorrelated surface punctuated by lakes (Figure 4a), intended to mimic Titan's polar landscape. It is generated by constructing a synthetic two-dimensional Fourier spectrum with a power law relationship between Fourier amplitude F and radial frequency f, $F \propto f^{-\beta}$, adding random perturbations to the amplitude and phase and taking the inverse Fourier transform [*Perron et al.*, 2008b]. The lowest 10% of elevations are designated as lakes, consistent with the approximate areal coverage of lakes in Titan's north polar region [*Aharonson* et al., submitted manuscript, 2013], and are assigned fixed elevations and treated as fluid and sediment mass sinks. Autocorrelation of the surface is controlled by varying β: A larger β gives a smoother surface with fewer local minima and maxima, while a smaller β creates a rough surface with many local minima and maxima. We use $\beta = 2.0$, which best reproduces the distribution of lakes in the north polar region and is consistent with the power spectral exponent estimated by *Sharma and Byrne*

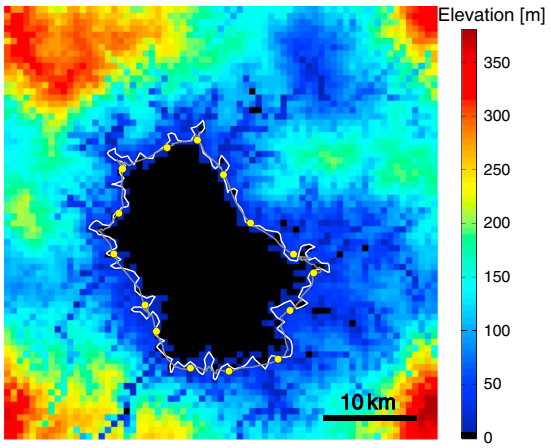

Figure 5. Illustration of procedure for measuring shoreline sinuosity. Background image is a coarsened landscape evolution model solution with colors indicating relative elevations. White line is the elevation contour taken 20 m above lake level. Gray line is the contour after smoothing by averaging. Yellow points represent the decimated version of the smoothed contour, which is used as an estimate of the contour shape prior to fluvial incision.

[2010], but we also test the sensitivity of our results to this parameter (see section 5.5).

[20] The model landscape evolves by solving equation (1) forward in time using an explicit finite difference method [*Perron et al*., 2008a, 2009, 2012]. Drainage area A is calculated at each iteration with the D∞ algorithm of *Tarboton* [1997], with local minima forced to "overflow," such that all points eventually drain into a lake. After each iteration, any slopes that exceed the threshold gradient are eroded until their gradients return to the threshold value. All the simulations analyzed in this paper were performed on a 50×50 km domain with periodic boundaries and a grid point spacing of 125 m in both the x and y directions. Initial relief, the difference between the maximum elevation and the lake level, was approximately 400 m. Each simulation was run for 1 Myr with an adaptive time step that ensured numerical stability and second-order accuracy. This time interval is not intended to match the actual duration of fluvial erosion on Titan, which is unknown, nor is the relief intended to match the actual topography of the polar regions. The initial relief, the run duration, and the magnitudes of K and m in equation (1) trade off in determining the amount of fluvial erosion that occurs over the course of a run. Neither the duration of fluvial erosion nor the values of K and m are known for Titan, so we focus our analysis on the amount of cumulative erosion relative to the initial relief rather than the absolute amount of erosion or the rate at which it occurs and simply choose a combination of run duration (1 Myr) and parameters ($K = 510^{-6}$ year^{-1}, $m = 0.5$) that produces extensive erosion of the initial topography over the course of a run. We set the value $m = 0.5$, which is consistent with typical values inferred from field observations on Earth [*Snyder et al*., 2000; *Perron and Royden*, 2013]. In section 5.5, we quantify the sensitivity of our results to the value of m and the statistical properties of the initial surface. As noted in section 3.2, the value of the threshold hillslope angle does not substantially influence the fluvial networks generated by the model.

[21] In the early stages of each simulation, small incipient valleys with few tributaries form at the lake margins (Figure 4b). As these valleys incise deeper, they propagate upslope and develop more extensive tributary networks (Figure 4c). Eventually, fluvial valleys fill the entire landscape, and drainage divides that began as broad local maxima are intensely dissected (Figure 4d). As fluvial incision produces a landscape of branching valleys interspersed with sharp ridgelines, elevation contours become progressively more sinuous. In section 3.4, we show how increasing contour sinuosity can be used as a proxy for cumulative erosion.

3.4. Relating Contour Sinuosity to Cumulative Erosion

[22] As noted in section 3.3, neither the relief nor the erosion rates are precisely known for Titan's polar regions, and therefore, the model results are not intended to match a specific time interval, erosion rate, or spatial scale. Instead, we seek a general, dimensionless relationship between relative erosion and the shapes of topographic contours around the lake margins.

[23] Several measures of contour shape correlate with the extent of fluvial erosion. In their comparison of lake shapes on Titan and Earth, *Sharma and Byrne* [2011] use the shorelines' fractal dimension [*Mandelbrot*, 1967] and the shoreline development index, the ratio of a shoreline's length to the circumference of a circle with the same area. Both of these are useful general measures of lake shape that are influenced by the increase in local curvature as fluvial valleys dissect the lake margins (Figure 4), but both have limitations when used as a proxy for erosion. For example, the shoreline development index is influenced by lake characteristics that are not related to fluvial processes, such as the overall noncircularity of the lake shape. We investigated the influence of fluvial erosion on the fractal dimensions of modeled shorelines and found the changes to be subtle relative to differences associated with initial topography, particularly when coarse spatial resolution makes it difficult to obtain a precise estimate of the spectral slope at short wavelengths. In contrast, we found that a simple measure of contour sinuosity, described below, is a more direct and reliable proxy for fluvial erosion.

[24] We ran the landscape evolution model for 20 different initial surfaces to average over the random variability in the resulting final surfaces. The final topographic surfaces were resampled by linear interpolation to the same resolution as the image used to map each contour or shoreline (see sections 4 and 5). We selected a contour 20 m above the lake level (5% of the total relief of the landscape) to simulate the flooded landscape of Titan and calculated the total contour length. The lengths of contours 15 and 25 m above the lake surface differed by approximately 4%, indicating that the results are not very sensitive to the sampled elevation. This contour was then smoothed by averaging the coordinates within a distance increment that is approximately equal to the width of the largest visible fluvial incision features around the lake margin. The smoothed contour is used as an estimate of the background shape of the lake. This smoothed contour is still artificially long because it contains the same number of points as the original unsmoothed contour, so the points are subsampled. We constructed the subsampled contour by retaining every 20th point, which we determined to be the minimum number of anchor points

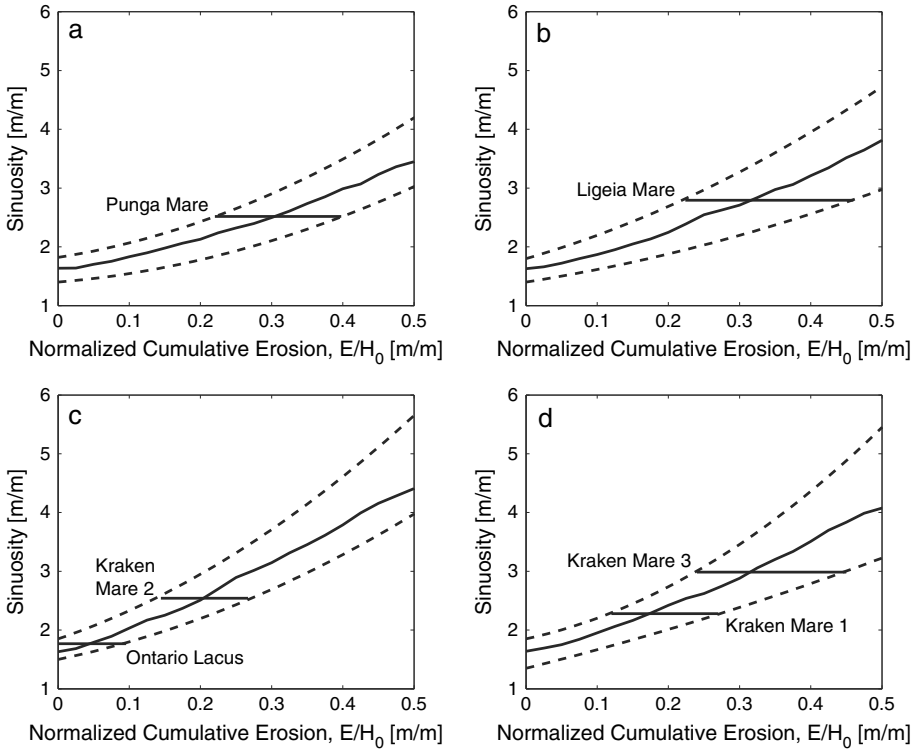

Figure 6. Calibration curves relating sinuosity to spatially averaged cumulative erosion for different shorelines on Titan. Separate calibration curves are required for different shorelines because SAR image resolution, which varies among shorelines, influences the measured sinuosity. Spatial resolution (the average spacing between mapped points) in kilometers is (a) 0.71, (b) 0.62, (c) 0.48, and (d) 0.54. In each panel, the solid curve represents the mean trend and dotted lines represent 95% confidence envelopes. Horizontal solid bars are placed at the measured sinuosity value of each shoreline. Intersections of the horizontal bars with the calibration curves and the dashed envelopes, respectively, represent the cumulative erosion estimates and the 95% confidence intervals. Confidence limits are estimated by binning the model data, calculating a 95% confidence ellipse for each bin to reflect uncertainty in both sinuosity and erosion, and fitting polynomial curves to the boundaries of the error ellipses.

required to represent the shape of the smoothed contour. This procedure is illustrated in Figure 5. The ratio of the mapped contour length to the length of the smoothed, downsampled contour is the contour sinuosity, S. This measure of sinuosity has the disadvantage of being resolution dependent, but we account for this in our procedure, as described below.

[25] The spatially averaged cumulative erosion, E, is calculated by taking the difference between the elevation field at any time during the simulation and the initial elevation field and averaging over the grid. To obtain a dimensionless measure of erosion, we then divide E by the relief of the initial elevation field, H_0 [*Black et al.*, 2012]. We calculated the sinuosity S at 20 instants in each model run, which corresponded to 20 values of E/H_0, to calibrate the relationship between these two quantities. We interpolated the data into 20 evenly spaced bins according to E/H_0 and calculated the mean S and 95% confidence interval within each bin. The means define the calibrated relationship between sinuosity and E/H_0, and the boundaries of the confidence envelope denote the uncertainty in this relationship.

[26] As noted above, a contour sinuosity measurement depends on the resolution of the data used to map the contour. This must be accounted for in our calibration, because the resolution of Cassini SAR images varies, and is not necessarily the same as the grid resolution of our model. We therefore constructed a separate model-derived sinuosity versus E/H_0 curve for each Titan lake shoreline (Figure 6) by downsampling the model topography to the corresponding SAR resolution. These coarsened model solutions are based on the average spacing of the measured points of each shoreline on Titan. The moderate differences among the curves in Figure 6 illustrate the magnitude of this resolution dependence. In section 5.5, we test the sensitivity of the sinuosity-erosion relationship to the fluvial incision parameters and the characteristics of the initial topography.

4. Testing the Sinuosity-Erosion Relationship With Terrestrial Data

[27] To test our procedure for estimating cumulative erosion, we compared our model-calibrated relationship between contour sinuosity and cumulative erosion with a terrestrial landscape where both quantities can be measured. We sought a study site where fluvial incision has produced significant drainage network development, but the initial surface could easily be reconstructed. We selected an area surrounding the Minnesota River in southern Minnesota, USA, which experienced a sudden drop in base level roughly

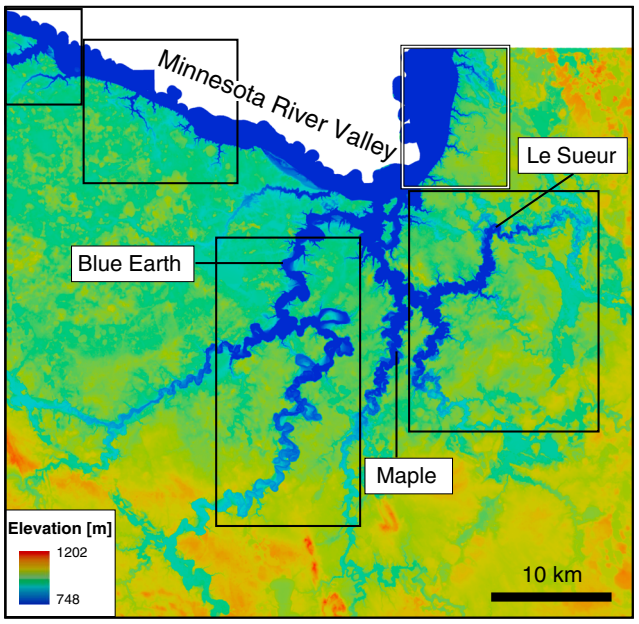

Figure 7. Elevation map of the study area adjacent to the Minnesota River Valley (wide blue feature at top of map) in southern Minnesota, USA, based on laser altimetry acquired and processed by the National Center for Airborne Laser Mapping. The major tributaries are the Blue Earth River, Maple River, and Le Sueur River. Boxes indicate areas analyzed to generate the points plotted in Figure 9. White box represents area shown in Figure 8.

13 ka when outburst floods from glacial Lake Agassiz caused tens of meters of incision in the Minnesota River valley [*Clayton and Moran*, 1982]. This base level drop triggered a wave of incision that propagated up several tributaries, including the Le Sueur, Maple, and Blue Earth Rivers, and into the surrounding plateau of glacial till and outwash (Figure 7). Many of the tills are overconsolidated and display mechanical properties more typical of rock than of sediment, such as brittle fracturing and high cohesion [*Gran et al.*, 2013]. The transiently incising channels show characteristics of detachment-limited fluvial incision, including propagation of a knickpoint roughly 40 km up the tributaries, which has created numerous strath terraces [*Belmont et al.*, 2011; *Gran et al.*, 2011, 2013]. *Gran et al.* [2013] considered the most appropriate model for describing the long-term incision and found that a transport-limited model (in which erosion rate depends on the downstream divergence of sediment flux) cannot preserve the slope break associated with the knickpoint. These observations suggest that the main stage of fluvial incision can be described with the model presented in section 3.1. The nearly horizontal remnants of the plateau surface and the acquisition of a high-resolution laser altimetry map (Figure 7) make it possible to measure both the volume eroded by the wave of fluvial incision [*Gran et al.*, 2009, 2011, 2013; *Belmont et al.*, 2011] and the sinuosity of topographic contours through the dissected plateau, creating an opportunity to test the model-derived relationship between erosion and sinuosity.

[28] We divided the margin of the plateau into five sections (Figure 7) and coarsened the topography in each section using the procedure described in section 3.4 to yield the same relative resolution (defined as the average horizontal spacing of elevation points divided by the length scale of the area of interest) as the SAR images of Titan's polar lakes. We used a relative resolution of 0.012, based on the values for the Titan study sites (see section 5). In each section, we measured the sinuosity of an elevation contour 20 m above the minimum elevation of the section. These contours trace out the fluvially dissected topography (Figure 8). We then approximated the initial plateau surface with a horizontal plane at the highest elevation in each section and estimated the cumulative erosion by measuring the depth of the modern surface beneath this plane. We also made this measurement for the entire area shown in Figure 7. In Figure 9, we compare these six paired measurements of contour sinuosity and erosion with the calibration curve generated from the landscape evolution model at the same relative resolution. All but one of the measurements fall within the 95% confidence intervals, and the measurement for the site as a whole lies very close to the mean trend. This comparison indicates that contour sinuosity is a useful proxy for spatially averaged fluvial erosion.

5. Application to Titan's Polar Regions

[29] The general relationship presented in section 3.4 provides a framework for estimating cumulative fluvial erosion in Titan's north polar landscape based on topographic contours from fluvially dissected lake margins. Since there are currently no digital elevation models with sufficient spatial coverage, resolution, or precision to make detailed measurements of the fluvially dissected topography around the polar lakes, we use SAR images to map lake shorelines that trace contours through drowned fluvial features.

5.1. SAR Data and Study Region

[30] The RADAR onboard the Cassini spacecraft operates at a wavelength of 2.17 cm and collects surface data on each

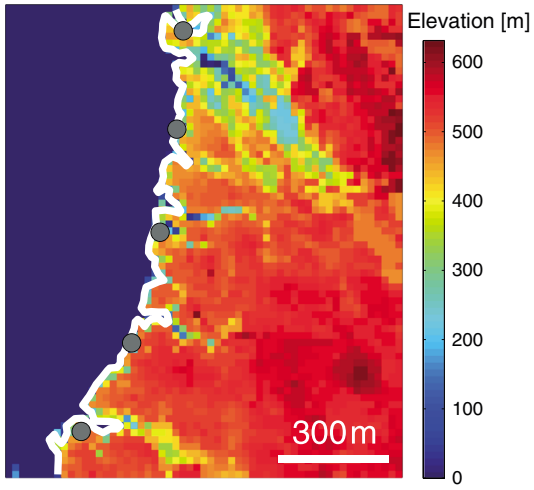

Figure 8. Coarsened DEM of Minnesota River study area outlined with white box in Figure 7, with colors indicating relative elevation. White line is the elevation contour 20 m above the lowest elevation in the area. Gray points represent the estimated original plateau margin shape reconstructed with the procedure described in section 3.4.

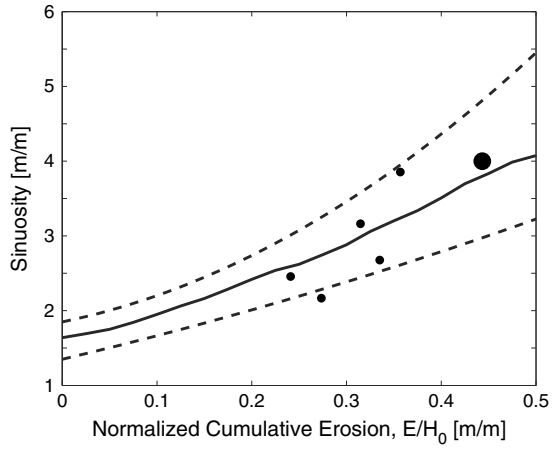

Figure 9. Calibration curve relating sinuosity to spatially averaged cumulative erosion, based on 20 landscape evolution model simulations, compared with topographic measurements for the study site adjacent to the Minnesota River (Figure 7). Solid and dashed lines were calculated as in Figure 6. Small circles correspond to the areas indicated in Figure 7. The large circle indicates the measurement for the entire study site.

Titan flyby while orbiting Saturn [*Elachi et al*., 2004]. The RADAR has four operational modes, of which Synthetic Aperture Radar (SAR) produces the highest-resolution images (300–1500 m/pixel). SAR brightness depends on the roughness, topographic slope, dielectric constant, and subsurface scattering of the terrain [*Stofan et al*., 2006; *Farr et al*., 2007]. In general, elevated terrain that is rough at the scale of the RADAR wavelength or contains surfaces with subresolution elements that face toward and away from the spacecraft appears radar bright, whereas smooth, nearly horizontal lake surfaces appear radar dark, making SAR images suitable for mapping lake shorelines. Strip-shaped SAR images, or swaths, taken during flybys have captured partial or complete shorelines of several large hydrocarbon lakes in the polar regions: Ligeia Mare, Kraken Mare, and Punga Mare in the north and Ontario Lacus in the south (Figures 10 and 11).

5.2. Test of Shoreline Identification Criterion

[31] Elevated levels of liquid hydrocarbons appear to have partially flooded valleys around the margins of these four large polar lakes [*Stofan et al*., 2007; *Wall et al*., 2010; *Aharonson* et al., submitted manuscript, 2013]. Assuming that each raised lake level defines a surface of constant gravitational potential, these elevated shorelines trace out contours through the fluvially dissected topography. We test the assumption that the bright-dark contrast visible in SAR images represents a fluid shoreline by examining altimetry profiles across lakes. One of the other Cassini RADAR modes is altimetry, which cannot operate at the same time as SAR, but one altimetry track does pass over Ontario Lacus and crosses the apparent shoreline at multiple points (Figure 11). We extracted the two nearest elevation points on either side of the first and last locations where the altimetry profile crosses the shoreline (Figure 11). The two groups of four points have mean elevations and standard deviations of 2574082 ± 1 m and 2574085 ± 4 m, and further analysis of the altimeter signal revealed a smooth surface with a root-mean-square height variation of less than 3 mm across each 100 m coherent resolution cell [*Wye et al*., 2009]. These very consistent elevations, combined with the generally level altimetry profile across Ontario Lacus, suggest that the bright-dark border visible in SAR images does represent an elevation contour.

5.3. Shoreline Mapping and Sinuosity Calculation

[32] Lake shorelines (Figures 10 and 11) were mapped manually in SAR images in a polar stereographic projection by digitizing points along the sharp boundary between light and dark areas. The spacing between adjacent points was typically 500 m, comparable to but slightly larger than the SAR image pixel size, but was wider in areas where the boundary was not as clear. In those areas, we placed shoreline points only where we were confident of the shoreline location, which required wider point spacing. We also compared our mapping with adjacent SAR swaths in which the contact was more sharply resolved and compared multiple overlapping swaths where they were available. Table 1 lists the average resolution at which each shoreline was mapped. In the north

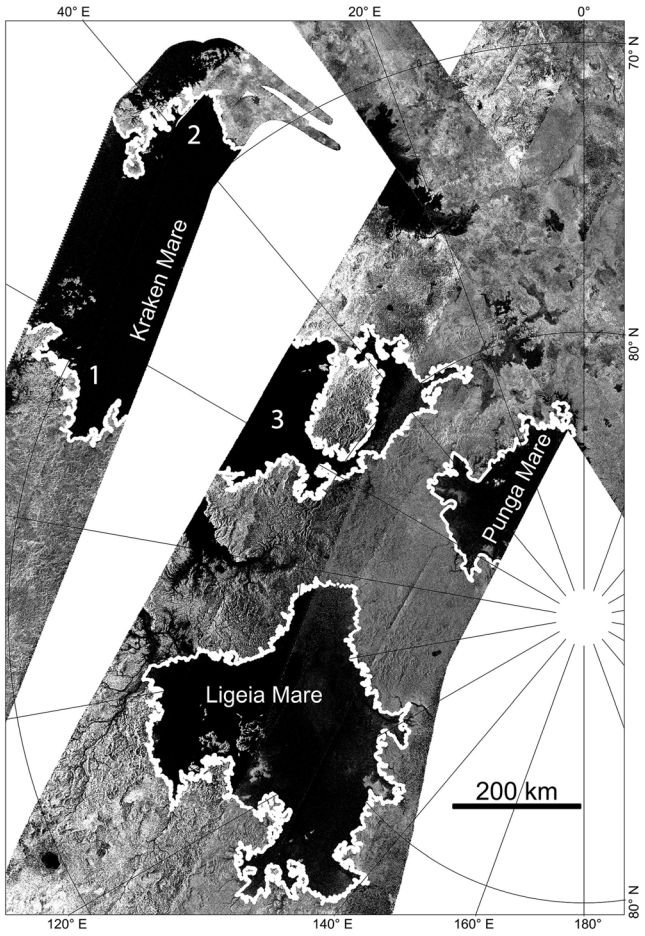

Figure 10. Stereographic projection of SAR image mosaic covering Titan's three major northern polar lakes (maria). Pixel values represent normalized radar cross section σ_0 in decibels, from −20 dB (black) to +0 dB (white). White lines are the mapped shorelines used in this study. Numbers in Kraken Mare label the three shoreline segments that were analyzed separately.

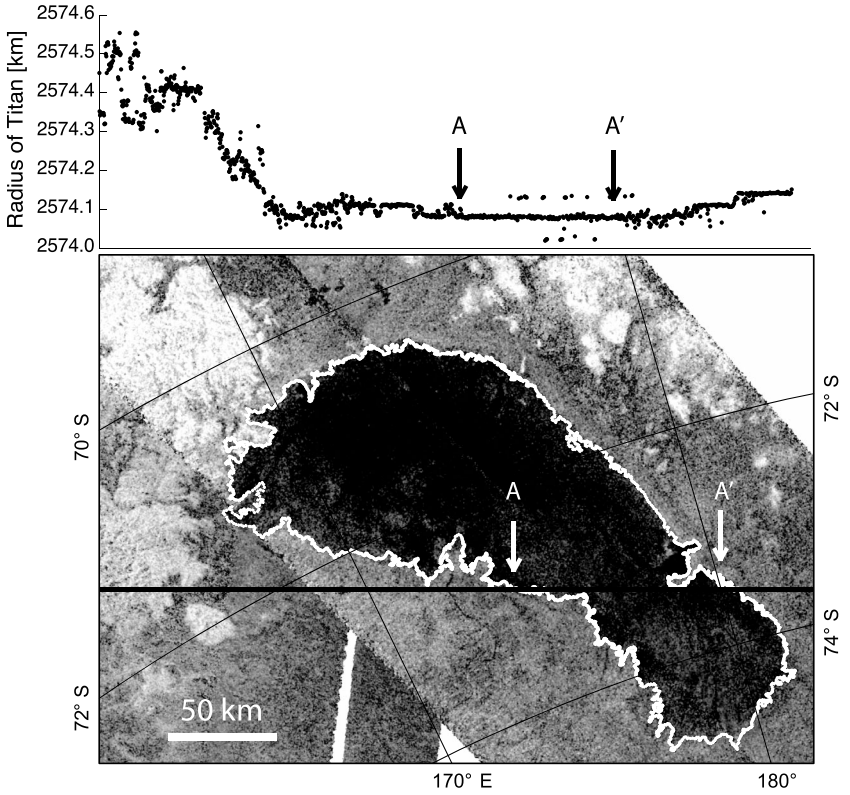

Figure 11. South polar stereographic projection of SAR images showing Ontario Lacus with altimetry profile plotted above. Pixel values represent normalized radar cross section σ_0 in decibels, from −20 dB (black) to +4 dB (white). The straight black line crossing the map indicates the orbit track, and the data points in the upper panel indicate the radius of Titan at the corresponding points on the surface. A and A′ mark the first and last locations where the altimetry track crosses the mapped shoreline.

polar region, we restricted our analysis to the maria (Punga, Ligeia, and Kraken). We mapped a single path around Ligeia Mare and the imaged section of Punga Mare. A closed contour of Kraken Mare has not yet been imaged at the time of this writing, so we mapped the three imaged sections of the main body of the lake (Figure 10) and analyzed these three contour segments separately. The section of Kraken Mare to the east of the section labeled 3 in Figure 10 was not analyzed because its shape appears to be so significantly influenced by fluvial topography that it is difficult to estimate a background shape.

[33] We calculated each shoreline's sinuosity in the same manner as described in section 3.4 for the landscape evolution model. Table 1 lists the resulting values. The sinuosity is between 2 and 3 for all the northern lakes, whereas Ontario Lacus in the south is considerably less sinuous, with $S = 1.77$.

5.4. Comparison With Model-Derived Erosion Proxy

[34] Using the measured sinuosity values S of the Titan shorelines (Table 1) and the model-generated calibration curves (Figure 6), we estimated the cumulative fluvial erosion in the areas surrounding the Titan shorelines. In Figure 6, we plot a horizontal bar corresponding to each measured Titan shoreline sinuosity. The intersection of each bar with the calibration curve for the corresponding spatial resolution yields an estimate of E/H_0, and the intersection of the bar with the 95% confidence bounds defines the confidence interval for the cumulative erosion estimate. The E/H_0 estimates and 95% confidence intervals are summarized in Table 1. In the north, we estimate that fluvial networks around Ligeia Mare, Punga Mare, and section 3 of Kraken Mare have eroded through roughly 30% of the initial relief, with a 95% confidence interval of roughly 20% to <50%. The shorter sections of Kraken Mare's shoreline yield somewhat smaller estimates of E/H_0: 17% (9%–33%) for Kraken Mare 1 and 20% (12%–33%) for Kraken Mare 2. In the south polar region, the less sinuous shoreline of Ontario Lacus implies an E/H_0 of only 4% (0%–14%). Thus, for the shorelines examined in this study, the best estimate of spatially averaged cumulative erosion falls between 17% and 31% for the north polar region but is only 4% for the one lake analyzed in the south polar region.

Table 1. Sinuosity and Cumulative Erosion Estimates for All Shorelines in the Study

Shoreline	Sinuosity	E/H_0	[a]Resolution (km)
Kraken 1	2.28	$0.17^{+0.08}_{-0.04}$	0.54
Kraken 2	2.54	$0.20^{+0.06}_{-0.06}$	0.48
Kraken 3	2.99	$0.31^{+0.13}_{-0.08}$	0.54
Ligeia	2.79	$0.31^{+0.14}_{-0.09}$	0.62
Punga	2.16	$0.30^{+0.09}_{-0.08}$	0.71
Ontario	1.77	$0.04^{+0.05}_{-0.04}$	0.48

[a]The average spacing between mapped points and the value used to coarsen the landscape evolution model output.

5.5. Sensitivity to Initial Conditions and Fluvial Incision Parameters

[35] As noted in section 3.3, the β value (the negative slope of the synthetic Fourier spectrum) used to generate the initial topographic surface controls the relative smoothness of the surface, and therefore the distribution of local minima. The distribution of minima in turn determines the size distribution of lakes in the simulation. All the model calculations presented above used $\beta = 2.0$. We tested the sensitivity of our results to initial conditions by constructing sinuosity-erosion calibration curves for $\beta = 1.7$ and 2.5, the extremes of the range of β values that produce a distribution of minima comparable to the size distribution of lakes on Titan. β values below 1.7 produce many small, irregularly shaped topographic minima scattered throughout the landscape, whereas values of β higher than 2.5 produce very smooth terrain with a single large, roughly circular sink, neither of which is consistent with the intermediate-sized, moderately irregularly shaped lakes that cover roughly 10% of the land area in Titan's north polar region [*Hayes et al*., 2008; *Aharonson* et al., submitted manuscript, 2013] (e.g., Figure 10). The results of this sensitivity test are presented in Figure 12. While the slope of the mean trend and the extent of the 95% confidence envelope do show some sensitivity to β, the mean trend is very consistent for $E/H_0 \approx 0.3$, the value estimated for most of the northern lakes analyzed here. The larger range of sinuosity for small values of E/H_0 implies that our estimate of the magnitude of erosion around Ontario Lacus is somewhat less certain, but either of the extreme values of β implies an E/H_0 of less than about 12%, which is still much smaller than the value for the northern lakes. We therefore conclude that these results (the magnitude of erosion in the north and the different extents of erosion between north and south) are relatively insensitive to the choice of initial topography.

[36] We also tested the sensitivity of our results to the parameter m in equation (1), which describes how fluid discharge and channel geometry vary downstream and which is the only tunable parameter in the fluvial incision model. For our study, we set $m = 0.5$, a typical value for detachment-limited terrestrial channels [e.g., *Snyder et al*., 2000; *Whipple and Tucker*, 1999]. We repeated our analysis with $m = 0.4$ and $m = 0.6$. A larger value of m indicates that flow discharge increases more rapidly with increasing drainage area or that channel width increases less rapidly with increasing discharge. Larger values of m produce more concave river longitudinal profiles. Comparison of the calibration curves and confidence envelopes for the three values of m (Figure 13) shows close agreement between $m = 0.4$ and $m = 0.5$, but somewhat higher values of E/H_0 for large contour sinuosity with $m = 0.6$. The mean trends for $E/H_0 < 0.2$, on the other hand, are very similar for all three values of m. The maximum sinuosity we measured is approximately 3 (for Kraken Mare section 3), which corresponds to $E/H_0 \approx 0.3$ for $m = 0.4$ and $m = 0.5$, compared with $E/H_0 \approx 0.38$ for $m = 0.6$. We therefore conclude that our results are only moderately sensitive to m. This assumes that m on Titan falls in the typical range of terrestrial values, which is likely if fluvial erosion on Titan is driven by open-channel flow fed by runoff [*Perron et al*., 2006; *Aharonson* et al., submitted manuscript, 2013; *Burr et al*., 2013].

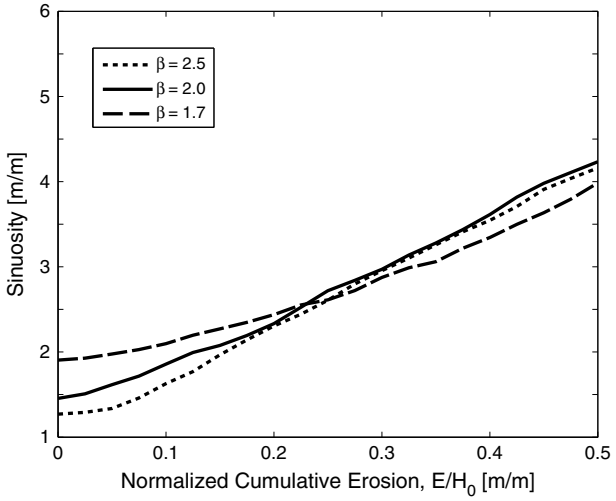

Figure 12. Sensitivity of the sinuosity-erosion calibration curve to β, the negative slope of the synthetic Fourier spectrum used to generate the random initial topography, at the resolution of Kraken Mare 1 and Ontario Lacus. Lines represent mean sinuosities at different values of β. Uncertainties are of comparable magnitude to those in Figure 6.

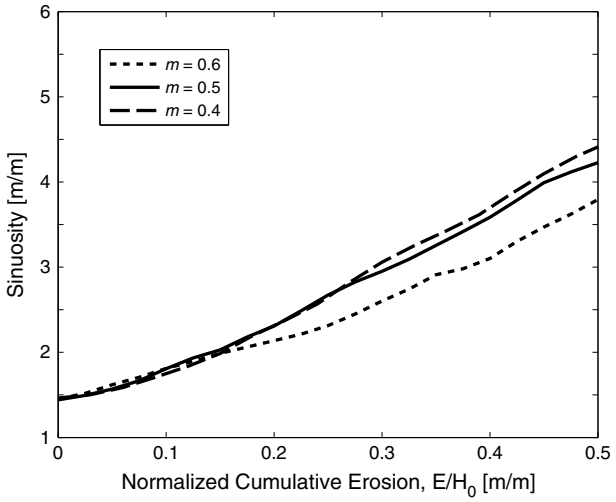

Figure 13. Sensitivity of the sinuosity-erosion calibration curve to m, the exponent on drainage area, A, in the fluvial incision term, at the resolution of Kraken Mare 1 and Ontario Lacus. Lines represent mean sinuosities at different values of m. Uncertainties are of comparable magnitude to those in Figure 6.

6. Discussion

6.1. Comparison With Previous Erosion Estimates

[37] The range of E/H_0 values estimated here for the northern lakes is somewhat larger than a previous estimate for the average fluvial erosion over a larger area in the north polar region. *Black et al*. [2012] used a relationship between fluvial network geometry and cumulative erosion to estimate E/H_0 for two north polar areas. They based their approach on the same landscape evolution model used here, so any differences between their erosion estimates and ours are not due to different assumed erosion laws. *Black et al*. [2012] estimated $0.4\% < E/H_0 < 9\%$ for fluvial networks south of Ligeia Mare

and $> 0.6\%$ (with no reliable upper bound) for fluvial networks between Ligeia Mare and Kraken Mare. Our measurement approach, which provides a localized estimate of erosion in areas immediately surrounding the lakes, complements the approach of *Black et al*. [2012], who estimated erosion from planform drainage network shapes covering larger areas in the north polar region. The difference between the two estimates suggests that fluvial dissection in Titan's north polar region is more extensive near the lake margins than in areas farther from the lakes, which is consistent with the interpretation that drainage networks have propagated upslope from the lake margins as fluvial erosion has acted on a rough initial surface. This is the expected sequence for transient, detachment-limited fluvial incision (Figure 4). Our estimate for cumulative erosion around Ontario Lacus is also consistent with a previous estimate of $0.5\% < E/H_0 < 16\%$ in a nearby region imaged in the T39 swath [*Black et al*., 2012].

6.2. Geographical Trends

[38] There is a clear difference between the amounts of estimated erosion around the northern lakes compared with Ontario Lacus in the south polar region (Figure 11 and Table 1). We estimate that rivers in the north have eroded through 17%–31% of the initial landscape, whereas the estimate for Ontario Lacus is only 4%. This estimate is consistent with the visual impression that the fluvial features near Ontario are less developed and fewer in number, such that the shoreline appears significantly smoother than the north polar lakes. However, it is also possible that this north-south difference is partly a consequence of less extensive flooding of fluvial topography in the south: Cassini has performed multiple flybys over Ontario Lacus and has observed receding lake levels [*Barnes et al*., 2009; *Moriconi et al*., 2010; *Wall et al*., 2010; *Hayes et al*., 2011; *Turtle et al*., 2011b] , which raises the possibility that more extensive fluvial dissection exists around the Ontario margin but is less apparent because the more dissected topography is not currently flooded.

[39] Within the northern polar region, the lakes analyzed here have similar estimated erosional values. Ligeia Mare, Punga Mare, and Kraken Mare 3 have E/H_0 values of 31%, 30%. and 31%, respectively, while Kraken Mare 1 (17%) and Kraken Mare 2 (20%) are somewhat lower. It is not clear if this is an artifact of the analysis on shorter sections of shoreline or if different parts of the Kraken margin have experienced different amounts of erosion. Even if there are systematic errors in the magnitudes of our erosion estimates, the relative differences in shoreline sinuosity should still provide an estimate of relative fluvial erosion. We therefore expect that the observation of similar overall extents of fluvial erosion around different major lakes in the north polar region is a robust result.

6.3. Implications for Polar Sediment and Volatile Budgets

[40] Most of the polar fluvial features terminate at lake margins, implying that most of the sediment produced by fluvial erosion is eventually deposited in the lakes. If the lake levels are set by the height of a regional subsurface hydrocarbon reservoir [*Hayes et al*., 2008; *Mitchell et al*., 2009], sediment accumulation in the lakes should have a minimal long-term effect on lake levels. If, on the other hand, lake levels are controlled by direct exchange of hydrocarbons between the surface and atmosphere, and if the sediment is insoluble in the liquid that fills the lakes [*Lorenz and Lunine*, 1996], the fluid displacement that occurs when sediment is deposited in the lakes would raise lake levels. The magnitude of the effect depends on the amount of erosion that has occurred and the ratio of the lake's area to its drainage basin area. For example, if the erosion has occurred over a basin about the same size as the lake itself, all eroded sediment was deposited in a steep-sided lake, and the topography had an initial relief of a few hundred meters, our erosion estimates of $E/H_0 \approx 0.2$ to 0.3 would imply that the lake level has risen approximately 100 m.

[41] If this effect is as significant as we estimate, it provides a possible nonclimatic explanation for the apparent rise in lake levels that has flooded fluvial topography in both the north and south polar regions. Estimates of lake volume changes based on observed lake level changes would need to take sediment displacement into account. Thus, fluvial erosion has implications for volatile exchange between Titan's surface, subsurface, and atmosphere that extend beyond signatures of atmospheric precipitation. This progressive rise in lake levels would be superimposed on any fluctuations associated with orbital variability [*Aharonson et al*., 2009].

[42] It is interesting to note that Ontario Lacus, where we estimate the least fluvial erosion has occurred, is observed to be experiencing a drop in lake level, whereas the north polar lakes where more erosion is inferred appear to have experienced more flooding around the lake margins. One possible interpretation is that more rapid and extensive fluvial erosion and lacustrine sediment deposition in the north polar region have raised lake levels faster than in the south, where slower erosion and sediment displacement have not kept pace with other factors that are slowly draining Ontario Lacus. However, the extent of flooding of lake margins may influence our erosion estimates by producing more sinuous shorelines when lake levels are higher, making it difficult to disentangle cause and effect. Thus, another possible interpretation of the hemispheric difference in shoreline sinuosities is that orbital variations [*Aharonson et al*., 2009] have lowered Ontario's surface to a level where it inundates a less incised and more alluviated portion of the lake margin, whereas higher levels in north polar lakes have flooded more incised valleys in which little aggradation has occurred.

6.4. Implications for Erosional Resurfacing on Titan

[43] One of our objectives in estimating the cumulative fluvial erosion of Titan's surface is to determine whether fluvial erosion might have been extensive enough to explain Titan's young surface age. Determining whether a topographic feature will be obscured by fluvial erosion is not as simple as comparing our spatially averaged estimates of E/H_0 with the relief of the feature, because erosion is concentrated in valleys and can also vary in the downstream direction. More detailed numerical experiments are therefore required.

[44] As a qualitative indicator of the potential for fluvial resurfacing, we performed a set of additional landscape evolution simulations in which the otherwise random initial surfaces included several impact craters with a range of

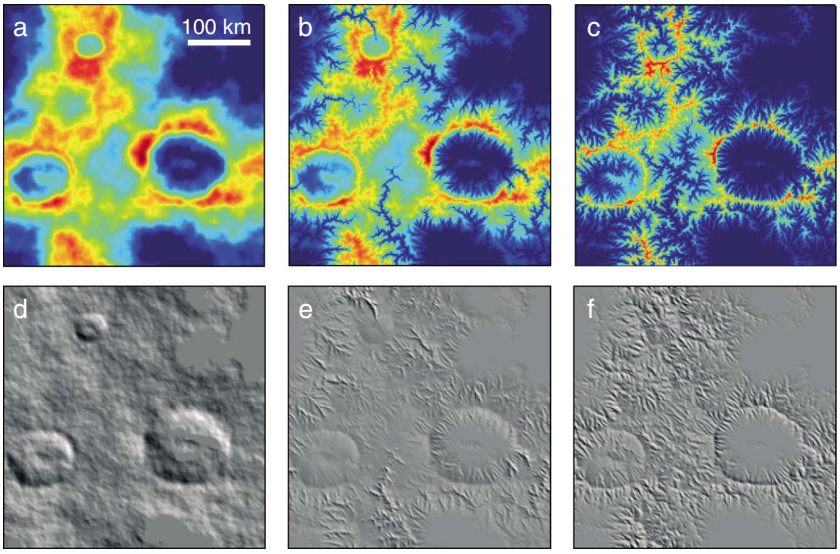

Figure 14. Landscape evolution model simulation of an eroding surface with three impact craters 50, 100, and 150 km in diameter. (a–c) Elevation is shown in color, with warmer colors representing higher elevations. (d–f) Shaded relief at a resolution of 1500 m/pixel, roughly equivalent to the coarsest Cassini SAR resolution. All panels are 400 × 400 km. Initial elevation range is 400 m. Topography is shown at normalized cumulative erosion values, E/H_0, of 0 (Figures 14a and 14d), 0.31 (Figures 14b and 14e), and 0.60 (Figures 14c and 14f).

diameters. We incorporate craters from the surface of Mars, mapped by the Mars Orbiter Laser Altimeter [*Smith et al*., 1999, 2001; *Neumann et al*., 2001], and scale them to the depths of similarly sized craters on Ganymede. Ganymede is a good proxy for fresh craters on Titan because both moons have similar gravity and surface composition, but since Ganymede does not have a thick atmosphere, the craters are relatively well preserved [*Schenk*, 1989; *Neish et al*., 2013]. We then examined the degree to which the craters remained visually recognizable after different amounts of cumulative erosion. Our estimates of fluvial resurfacing of these synthetic landscapes should be considered somewhat conservative: No sediment aggradation occurs in the model, so features such as craters are erased only by eroding them away, not by filling them in.

[45] Figure 14 shows the model elevations (Figures 14a–14c) as well as shaded relief maps based on model topography that has been coarsened to the approximate resolution of SAR images (Figures 14d–14f), for different stages in a representative simulation. We use shaded relief maps as a rough approximation for the appearance of topography in a SAR image [*Black et al*., 2012; *Burr et al*., 2013], because incidence angle is a major control on SAR backscatter. At $E/H_0 = 0.31$, the largest average amount of cumulative erosion inferred from our study of the polar lakes (Table 1); all three craters are still clearly visible even in the coarsened shaded relief (Figure 14e). Only once E/H_0 exceeds approximately 0.60 do smaller craters become difficult to recognize in the coarsened data (Figure 14f). Again, we emphasize that sediment aggradation on crater floors or in other closed depressions could make craters more difficult to recognize than Figure 14 suggests. Nonetheless, the observation that crater rims are far from being obliterated after the amount of erosion we have estimated around Titan's polar lakes leads us to suggest that fluvial erosion alone may not have been sufficient to create Titan's geologically young surface, at least in the polar regions studied here.

7. Conclusions

[46] We estimated the cumulative fluvial erosion around several lake margins in the polar regions of Titan by comparing the sinuosity of topographic contours defined by flooded landscapes surrounding Titan's polar lakes to contours produced by a simple landscape evolution model. We find that the north polar lakes in our analysis have eroded through approximately 17% to 31% of the initial relief of the landscape, whereas the single south polar lake in our analysis has eroded through approximately 4% of the initial relief. These estimates complement previous studies of erosion over larger areas in the north polar region and suggest that the headward propagation of drainage networks has left lake margins more extensively dissected than highlands further away from the lakes. These erosion estimates also provide a basis for assessing whether fluvial erosion of topographic features such as impact craters could explain the young apparent age of Titan's surface. Synthetic impact craters in landscape evolution simulations are still visible at SAR resolution even after 30% of the initial relief has been eroded, suggesting that while fluvial erosion has clearly modified Titan's surface, additional erosional and depositional processes may be required to explain the extent of resurfacing on Titan.

[47] **Acknowledgments.** This work was supported by a Robert R. Shrock Graduate Fellowship to Yodit Tewelde and by NASA Cassini Data Analysis Program award NNX09AE73G to Peter Ford. We thank Randy Kirk and Larry Soderblom for making the Huygens orthoimages and DEM publicly available, and Trent Hare for assistance with the data. We gratefully acknowledge the Cassini Radar Team and all those who have worked on the Cassini-Huygens mission. We also thank Patrick Belmont and Noah Finnegan for assistance with the Minnesota River laser altimetry data. Reviews by Devon Burr and an anonymous reviewer helped us improve the manuscript.

References

Aharonson, O., A. G. Hayes, J. I. Lunine, R. D. Lorenz, M. D. Allison, and C. Elachi (2009), An asymmetric distribution of lakes on Titan as a possible consequence of orbital forcing, *Nat. Geosci.*, *2*(12), 851–854, doi:10.1038/ngeo698.

Barnes, J. W., et al. (2009), Shoreline features of Titan's Ontario Lacus from Cassini/VIMS observations, *Icarus*, *201*(1), 217–225, doi:10.1016/j.icarus.2008.12.028.

Belmont, P., et al. (2011), Large shift in source of fine sediment in the upper Mississippi River, *Environ. Sci. Technol.*, *45*(20), 8804–8810, doi:10.1021/es2019109.

Bierman, P. R. (1994), Using in situ produced cosmogenic isotopes to estimate rates of landscape evolution: A review from the geomorphic perspective, *J. Geophys. Res.*, *99*(B7), 13,885–13,896, doi:10.1029/94JB00459.

Binnie, S. A., W. M. Phillips, M. A. Summerfield, and L. K. Fifield (2007), Tectonic uplift, threshold hillslopes, and denudation rates in a developing mountain range, *Geology*, *35*(8), 743–746, doi:10.1130/G23641A.1.

Black, B. A., J. T. Perron, D. M. Burr, and S. A. Drummond (2012), Estimating erosional exhumation on Titan from drainage network morphology, *J. Geophys. Res.*, *117*, E08006, doi:10.1029/2012JE004085.

Burr, D., et al. (2013), Fluvial features on Titan: Insights from morphology and modeling, *Geol. Soc. Am. Bull.*, *125*(3–4), 299–321, doi:10.1130/B30612.1.

Burr, D. M., J. P. Emery, R. D. Lorenz, G. C. Collins, and P. A. Carling (2006), Sediment transport by liquid surficial flow: Application to Titan, *Icarus*, *181*, 235–242.

Burr, D. M., R. E. Jacobsen, D. L. Roth, C. B. Phillips, K. L. Mitchell, and D. Viola (2009), Fluvial network analysis on Titan: Evidence for subsurface structures and west-to-east wind flow, southwestern Xanadu, *Geophys. Res. Lett.*, *36*, L22203, doi:10.1029/2009GL040909.

Clayton, L., and S. R. Moran (1982), Chronology of Late Wisconsinan glaciation in middle North America, *Quat. Sci. Rev.*, *1*, 55–82.

Collins, G. C. (2005), Relative rates of fluvial bedrock incision on Titan and Earth, *Geophys. Res. Lett.*, *32*, L22202, doi:10.1029/2005GL024551.

Cornet, T., et al. (2012), Geomorphological significance of Ontario Lacus on Titan: Integrated interpretation of Cassini VIMS, ISS and RADAR data and comparison with the Etosha Pan (Namibia), *Icarus*, *218*(2), 788–806, doi:10.1016/j.icarus.2012.01.013.

Elachi, C., et al. (2004), Radar: The Cassini Titan radar mapper, *Space Sci. Rev.*, *115*(1–4), 71–110, doi:10.1007/s11214-004-1438-9.

Farr, T. G., et al. (2007), The Shuttle Radar Topography Mission, *Rev. Geophys.*, *45*, RG2004, doi:10.1029/2005RG000183.

Ferrier, K. L., K. L. Huppert, and J. T. Perron (2013a), Climatic control of bedrock river incision, *Nature*, *496*, 206–9, doi:10.1038/nature11982.

Ferrier, K. L., J. T. Perron, S. Mukhopadhyay, M. Rosener, J. D. Stock, K. L. Huppert, and M. Slosberg (2013b), Covariation of climate and long-term erosion rates across a steep rainfall gradient on the Hawaiian island of Kaua'i, *Geol. Soc. Am. Bull.*, *125*, 1146–1163, doi:10.1130/B30726.1.

Gran, K. B., P. Belmont, S. S. Day, C. Jennings, A. Johnson, L. Perg, and P. R. Wilcock (2009), Geomorphic evolution of the Le Sueur River Minnesota, USA, and implications for current sediment loading, *Geol. Soc. Am. Spec. Pap.*, *451*, 119–130, doi:10.1130/2008.2451(08).

Gran, K. B., P. Belmont, S. S. Day, N. Finnegan, C. Jennings, J. W. Lauer, and P. R. Wilcock (2011), Landscape evolution in south-central Minnesota and the role of geomorphic history on modern erosional processes, *Geol. Soc. Am. Today*, *21*(9), 7–9, doi:10.1130/G121A.1.

Gran, K. B., N. J. Finnegan, A. L. Johnson, P. Belmont, C. Wittkop, and T. Rittenour (2013), Landscape evolution, valley excavation, and terrace development following abrupt postglacial base level fall, *Geol. Soc. Am. Bull.*, doi:10.1130/B30772.1.

Griffith, C. A., T. Owen, T. R. Geballe, J. Rayner, and P. Rannou (2003), Evidence for the exposure of water ice on Titan's surface, *Science*, *300*(5619), 628–30, doi:10.1126/science.1081897.

Hayes, A., et al. (2008), Hydrocarbon lakes on Titan: Distribution and interaction with a porous regolith, *Geophys. Res. Lett.*, *35*, L09204, doi:10.1029/2008GL033409.

Hayes, A. G., et al. (2011), Transient surface liquid in Titan's polar regions from Cassini, *Icarus*, *211*(1), 655–671, doi:10.1016/j.icarus.2010.08.017.

Howard, A. D. (1994), A detachment-limited model of drainage basin evolution, *Water Resour. Res.*, *30*(7), 2261–2285.

Howard, A. D., W. E. Dietrich, and M. A. Seidl (1994), Modeling fluvial erosion on regional to continental scales, *J. Geophys. Res.*, *99*(B7), 13,971–13,986.

Howard, A. D., and G. Kerby (1983), Channel changes in badlands, *Geol. Soc. Am. Bull.*, *94*(6), 739–752.

Jaumann, R., et al. (2008), Fluvial erosion and post-erosional processes on Titan, *Icarus*, *197*(2), 526–538, doi:10.1016/j.icarus.2008.06.002.

Kirk, R. L., E. Howington-Kraus, B. W. Stiles, S. Hensley, and the Cassini RADAR Team (2008), Digital topographic models of Titan produced by radar stereogrammetry with a rigorous sensor model, Lunar and Planetary Institute Science Conference Abstracts. Lunar and Planetary Inst. Technical Report, vol. 39, abstract 2320.

Kirk, R. L., et al. (2009), Three-dimensional views of Titan's diverse surface features from Cassini RADAR stereogrammetry, Lunar and Planetary Institute Science Conference Abstracts. Lunar and Planetary Inst. Technical Report, vol. 40, abstract 1413.

Kleinhans, M. G., H. Markies, S. J. de Vet, A. C. in 't Veld, and F. N. Postema (2011), Static and dynamic angles of repose in loose granular materials under reduced gravity, *J. Geophys. Res.*, *116*, E11004, doi:10.1029/2011JE003865.

Langhans, M. H., et al. (2012), Titan's fluvial valleys: Morphology, distribution, and spectral properties, *Planet. Space Sci.*, *60*(1), 34–51, doi:10.1016/j.pss.2011.01.020.

Le Gall, A., M. A. Janssen, P. Paillou, R. D. Lorenz, and S. D. Wall (2010), Radar-bright channels on Titan, *Icarus*, *207*, 948–958, doi:10.1016/j.icarus.2009.12.027.

Lopes, R. M. C., et al. (2007a), Cryovolcanic features on Titan's surface as revealed by the Cassini Titan Radar Mapper, *Icarus*, *186*(2), 395–412, doi:10.1016/j.icarus.2006.09.006.

Lopes, R. M. C., et al. (2007b), The lakes and seas of Titan, *Eos Trans. AGU*, *88*(51), 569–570, doi:10.1029/2007EO510001.

Lopes, R. M. C., et al. (2013), Cryovolcanism on Titan: New results from Cassini RADAR and VIMS, *J. Geophys. Res. Planets*, *118*, 416–435, doi:10.1002/jgre.20062.

Lorenz, R. D., and J. I. Lunine (1996), Erosion on Titan: Past and present, *Icarus*, *122*(1), 79–91, doi:10.1006/icar.1996.0110.

Lorenz, R. D., et al. (2007), Titan's young surface: Initial impact crater survey by Cassini RADAR and model comparison, *Geophys. Res. Lett.*, *34*, L07204, doi:10.1029/2006GL028971.

Lorenz, R. D., et al. (2008), Fluvial channels on Titan: Initial Cassini RADAR observations, *Planet. Space Sci.*, *56*(8), 1132–1144, doi:10.1016/j.pss.2008.02.009.

Lunine, J. I., and R. D. Lorenz (2009), Rivers, lakes, dunes, and rain: Crustal processes in Titan's methane cycle, *Annu. Rev. Earth Planet. Sci.*, *37*(1), 299–320, doi:10.1146/annurev.earth.031208.100142.

Mandelbrot, B. (1967), How long is the coast of Britain? Statistical self-similarity and fractional dimension, *Science*, *156*(3775), 636–638, doi:10.1126/science.156.3775.636.

McKay, C. P., A. Coustenis, R. Samuelson, M. Lemmon, R. Lorenz, M. Cabane, P. Rannou, and P. Drossart (2001), Physical properties of the organic aerosols and clouds on Titan, *Planet. Space Sci.*, *49*(1), 79–99, doi:10.1016/S0032-0633(00)00051-9.

Mitchell, K., R. Lopes, J. Radebaugh, E. R. Stofan, S. D. Wall, J. Kargel, R. Kirk, J. Lunine, S. Ostro, and T. Farr (2008), The formation of high latitude karst lakes on Titan and implications for the existence of polar caps, Lunar and Planetary Institute Science Conference Abstracts. Lunar and Planetary Inst. Technical Report, vol. 39, abstract 2170.

Mitchell, K. L., et al. (2009), A global subsurface alkanofer system on Titan? Lunar and planetary institute science conference abstracts. Lunar and Planetary Inst. Technical Report, vol. 40, abstract 1966.

Mitri, G., A. P. Showman, J. I. Lunine, and R. D. Lorenz (2007), Hydrocarbon lakes on Titan, *Icarus*, *186*(2), 385–394, doi:10.1016/j.icarus.2006.09.004.

Moriconi, M. L., J. I. Lunine, A. Adriani, E. D'Aversa, A. Negrão, G. Filacchione, and A. Coradini (2010), Characterization of Titan's Ontario Lacus region from Cassini/VIMS observations, *Icarus*, *210*(2), 823–831, doi:10.1016/j.icarus.2010.07.023.

Neish, C. D., R. L. Kirk, R. D. Lorenz, V. J. Bray, P. Schenk, B. W. Stiles, E. Turtle, K. Mitchell, and A. Hayes (2013), Crater topography on Titan: Implications for landscape evolution, *Icarus*, *223*(1), 82–90, doi:10.1016/j.icarus.2012.11.030.

Neish, C. D., and R. D. Lorenz (2012), Titan's global crater population: A new assessment, *Planet. Space Sci.*, *60*, 26–33.

Neumann, G. A., D. D. Rowlands, F. G. Lemoine, D. E. Smith, and M. T. Zuber (2001), Crossover analysis of Mars Orbiter Laser Altimeter data, *J. Geophys. Res.*, *106*(E10), 23,753–23,768, doi:10.1029/2000JE001381.

Niemann, H. B., et al. (2005), The abundances of constituents of Titan's atmosphere from the GCMS instrument on the Huygens probe, *Nature*, *438*(7069), 779–784, doi:10.1038/nature04122.

Pelletier, J. D. (2004), Persistent drainage migration in a numerical landscape evolution model, *Geophys. Res. Lett.*, *31*, L20501, doi:10.1029/2004GL020802.

Perron, J. T., and L. Royden (2013), An integral approach to bedrock river profile analysis, *Earth Surf. Processes Landforms*, *38*(6), 570–576, doi:10.1002/esp.3302.

Perron, J. T., M. P. Lamb, C. D. Koven, I. Y. Fung, E. Yager, and M. Ádámkovics (2006), Valley formation and methane precipitation rates on Titan, *J. Geophys. Res.*, *111*, E11001, doi:10.1029/2005JE002602.

Perron, J. T., W. E. Dietrich, and J. W. Kirchner (2008a), Controls on the spacing of first-order valleys, *J. Geophys. Res.*, *113*, F04016, doi:10.1029/2007JF000977.

Perron, J. T., J. W. Kirchner, and W. E. Dietrich (2008b), Spectral signatures of characteristic spatial scales and nonfractal structure in landscapes, *J. Geophys. Res.*, *113*, F04003, doi:10.1029/2007JF000866.

Perron, J. T., J. W. Kirchner, and W. E. Dietrich (2009), Formation of evenly spaced ridges and valleys, *Nature*, *460*, 502–505, doi:10.1038/nature08174.

Perron, J. T., P. W. Richardson, K. L. Ferrier, and M. Lapôtre (2012), The root of branching river networks, *Nature*, *492*, 100–103, doi:10.1038/nature11672.

Radebaugh, J., R. D. Lorenz, R. L. Kirk, J. I. Lunine, E. R. Stofan, R. M. C. Lopes, and S. D. Wall (2007), Mountains on Titan observed by Cassini Radar, *Icarus*, *192*(1), 77–91, doi:10.1016/j.icarus.2007.06.020.

Radebaugh, J., et al. (2008), Dunes on Titan observed by Cassini Radar, *Icarus*, *194*(2), 690–703, doi:10.1016/j.icarus.2007.10.015.

Schenk, P. (1989), Crater formation and modification on the icy satellites of Uranus and Saturn: Depth/diameter and central peak occurrence, *J. Geophys. Res.*, *94*(B4), 3813–3832.

Seidl, M. A., and W. E. Dietrich (1992), The problem of channel erosion into bedrock, *Catena Suppl.*, *23*, 101–124.

Sharma, P., and S. Byrne (2010), Constraints on Titan's topography through fractal analysis of shorelines, *Icarus*, *209*(2), 723–737, doi:10.1016/j.icarus.2010.04.023.

Sharma, P., and S. Byrne (2011), Comparison of Titan's north polar lakes with terrestrial analogs, *Geophys. Res. Lett.*, *38*, L24203, doi:10.1029/2011GL049577.

Smith, D. E., M. T. Zuber, S. C. Solomon, R. J. Phillips, J. W. Head, J. B. Garvin , W. B. Banerdt, D. O. Muhleman, G. H. Pettengill, and G. A. Neumann (1999), The global topography of Mars and implications for surface evolution, *Science*, *284*(5419), 1495–1503, doi:10.1126/science.284.5419.1495.

Smith, D. E., M. T. Zuber, H. V. Frey, J. B. Garvin, J. W. Head, and D. O. Muhleman (2001), Mars Orbiter Laser Altimeter: Experiment summary after the first year of global mapping of Mars, *J. Geophys. Res.*, *106*(2000), 689–722.

Snyder, N., K. Whipple, G. Tucker, and D. Merritts (2000), Landscape response to tectonic forcing: Digital elevation model analysis of stream profiles in the Mendocino triple junction region, northern California, *Geol. Soc. Am. Bull.*, *112*(8), 1250–1263.

Soderblom, L. A., et al. (2007), Topography and geomorphology of the Huygens landing site on Titan, *Planet. Space Sci.*, *55*(13), 2015–2024, doi:10.1016/j.pss.2007.04.015.

Sotin, C., et al. (2005), Release of volatiles from a possible cryovolcano from near-infrared imaging of Titan, *Nature*, *435*(7043), 786–789, doi:10.1038/nature03596.

Stiles, B. W., et al. (2009), Determining Titan surface topography from Cassini SAR data, *Icarus*, *202*(2), 584–598, doi:10.1016/j.icarus.2009.03.032.

Stofan, E. R., et al. (2006), Mapping of Titan: Results from the first Titan radar passes, *Icarus*, *185*, 443–456, doi:10.1016/j.icarus.2006.07.015.

Stofan, E. R., et al. (2007), The lakes of Titan, *Nature*, *445*(7123), 61–64, doi:10.1038/nature05438.

Tarboton, D. (1997), A new method for the determination of flow directions and upslope areas in grid digital elevation models, *Water Resour. Res.*, *33*(2), 309–319.

Tomasko, M. G., et al. (2005), Rain, winds and haze during the Huygens probe's descent to Titan's surface, *Nature*, *438*(7069), 765–778, doi:10.1038/nature04126.

Tucker, G., and G. Hancock (2010), Modelling landscape evolution, *Earth Surf. Processes Landforms*, *50*, 28–50, doi:10.1002/esp.1952.

Tucker, G. E., and R. L. Slingerland (1994), Erosional dynamics, flexural isostasy, and long-lived escarpments: A numerical modeling study, *J. Geophys. Res.*, *99*(B6), 12229, doi:10.1029/94JB00320.

Tucker, G. E., and R. Slingerland (1996), Predicting sediment flux from fold and thrust belts, *Basin Res.*, *8*(3), 329–349, doi:10.1046/j.1365-2117.1996.00238.x.

Turtle, E. P., A. D. Del Genio, J. M. Barbara, J. E. Perry, E. L. Schaller, A. S. McEwen, R. A. West, and T. L. Ray (2011a), Seasonal changes in Titan's meteorology, *Geophys. Res. Lett.*, *38*, L03203, doi:10.1029/2010GL046266.

Turtle, E. P., J. E. Perry, A. G. Hayes, and A. S. McEwen (2011b), Shoreline retreat at Titan's Ontario Lacus and Arrakis Planitia from Cassini Imaging Science Subsystem observations, *Icarus*, *212*(2), 957–959, doi:10.1016/j.icarus.2011.02.005.

Wall, S., et al. (2010), Active shoreline of Ontario Lacus, Titan: A morphological study of the lake and its surroundings, *Geophys. Res. Lett.*, *37*, L05202, doi:10.1029/2009GL041821.

Wasiak, F. C., D. Androes, D. G. Blackburn, J. A. Tullis, V. F. Chevrier, and J. Dixon (2013), A geological characterization of Ligeia Mare in the northern polar region of Titan, *Planet. Space Sci.*, *84*, 141–147, doi:10.1016/j.pss.2013.05.007.

Whipple, K. X., G. S. Hancock, and R. S. Anderson (2000), River incision into bedrock: Mechanics and relative efficacy of plucking, abrasion, and cavitation, *Geol. Soc. Am. Bull.*, *112*(3), 490–503.

Whipple, K. X., and G. E. Tucker (1999), Dynamics of the stream-power river incision model: Implications for height limits of mountain ranges, landscape response timescales, and research needs, *J. Geophys. Res.*, *104*(B8), 661–674, doi:10.1029/1999JB900120.

Willgoose, G. (2005), Mathematical modeling of whole landscape evolution, *Annu. Rev. Earth Planet. Sci.*, *33*(1), 443–459, doi:10.1146/annurev.earth.33.092203.122610.

Wood, C. A., R. Lorenz, R. Kirk, R. Lopes, K. Mitchell, E. Stofan, and The Cassini Radar Team (2010), Impact craters on Titan, *Icarus*, *206*, 334–344.

Wye, L. C., H. A. Zebker, and R. D. Lorenz (2009), Smoothness of Titan's Ontario Lacus: Constraints from Cassini RADAR specular reflection data, *Geophys. Res. Lett.*, *36*, L16201, doi:10.1029/2009GL039588.

Yung, Y. L., M. Allen, and J. P. Pinto (1984), Photochemistry of the atmosphere of Titan: Comparison between model and observations, *Astrophys. J. Suppl. Ser.*, *55*, 465–506, doi:10.1086/190963.